Article

Equilibrium, Kinetic and Thermodynamic Studies for the Adsorption of Metanil Yellow Using Carbonized Pistachio Shell-Magnetic Nanoparticles

Adnan [1,*], Muhammad Omer [1,*], Behramand Khan [2], Inkisar Khan [1], Muhammad Alamzeb [3], Farah Muhammad Zada [1], Ihsan Ullah [1], Rahim Shah [1], Mohammed Alqarni [4] and Jesus Simal-Gandara [5]

1   Institute of Chemical Sciences, University of Swat, Swat 19130, Khyber Pakhtunkhwa, Pakistan
2   Department of Chemistry, Islamia College University, Peshawar 25120, Khyber Pakhtunkhwa, Pakistan
3   Department of Chemistry, University of Kotli, Kotli 11100, Azad Jammu & Kashmir, Pakistan
4   Department of Pharmaceutical Chemistry, College of Pharmacy, Taif University, P.O. Box 11099, Taif 21944, Saudi Arabia
5   Nutrition and Bromatology Group, Department of Analytical Chemistry and Food Science, Faculty of Science, Universidade de Vigo, E-32004 Ourense, Spain
*   Correspondence: adnanchem@yahoo.com or adnanchem@uswat.edu.pk (A.); omarmarwat@uswat.edu.pk (M.O.)

Abstract: The cost-effective adsorbents of carbonized pistachio shell magnetic nanoparticles (CPSM-NPs) were synthesized. SEM, EDX, and BET characterized the prepared CPSMNPs. The CPSMNPs were used as adsorbents to remove Metanil Yellow (MY) dye. The adsorption of MY was investigated with the effect of pH, contact time, initial dye concentration, adsorbent dose, and temperature. The SEM image of CPSMNPs reveals fine particles with an average size of 400–700 nm and a substantial surface area increase ($112.58 \ \mathrm{m^2/g}$). The EDX analysis confirms the carbonization of PS to CPS and the successful impregnation of Fe_3O_4 nanoparticles. CPSMNPs showed excellent adsorption efficiency, i.e., 94% for adsorption of MY of 10 mL of 100 ppm MY at optimum conditions. Kinetics data fit pseudo-second-order kinetics. The Langmuir isotherm better represents the equilibrium data with the spontaneous sorption process. This study investigates that the synthesized nanoparticles have an excellent texture and can be used as a special adsorbent for the adsorption of wastewater pollutants like MY.

Keywords: pistachio shell; magnetic nanoparticles; adsorption; metanil yellow; adsorption isotherm; adsorption kinetic; thermodynamic; water cleaning

1. Introduction

Waterborne diseases due to wastewater are the central concern of today's world [1]. Wastewater of dyes excretes by various industries causes different copious diseases in humans and aquatic life [2,3]. Dyes substances are used in many industries, such as leather, textile, paper, paint, pesticides [1], etc. It has been reported that industries release 7×10^5 tons of waste dyes into the water every year [4,5]. These dyes are soluble in water; even their small quantity is visible in the water, deteriorating the quality. The dyes released into the water kill living things [6,7]. Some have mutagenic [8] and carcinogenic effects like benzidine or aryl amine dye [9,10].

Among the toxic dyes, one of them is metanil yellow (MY), also called acid yellow 36 (AY36), which is (3-(4-anilinophenylazo) benzene sulfonic acid sodium salts, an azo dye. MY is usually used in nutrition, pharmaceuticals, printing and dyeing, textile manufacturing, coloring and staining of woolen products, leather tanning, paper, pesticide, and plastic manufacturing [1,11–13], etc. MY is also a pH indicator ranging from 1.2–2.3 [14,15]. MY is toxic; its carcinogenic effect and mutagenic properties [16,17]. Toxicity of MY decreases the rate of spermatogenesis in animal bodies [18]. Due to its toxicity, it also

causes methemoglobinemia and cyanosis in humans on oral consumption. MY also cause enzymic and intestinal diseases in the human body [19]. In direct contact, it causes skin allergy [20]. MY is highly soluble with unlawful color but still used in the coloring of sweets, meat, ice creams, beverages, and soft drinks. Because of its yellow color, it is used for turmeric coating [14,15]. Thus, the elimination of these dyes wastes is needed for the day.

There are numerous strategies for removing dyes from wastewater effluents, i.e., filtration, coagulation, flocculation, microbial, biological degradation, electrochemical degradation [2,21], chemical oxidation, photo-catalytic degradation, and removal of the dye using adsorption [2,9]. These methods have associated problems such as using large amounts of chemicals [9]; filtration requires high energy; coagulation and flocculation produce a large amount of concentrated sludge. Microbial and biological degradation produce sludge and uncontrollable products. It might be practical for a smaller amount of dyes but cannot be applied on a large scale. Thus, electrochemical degradation requires high investment and needed high electrical supply [22]. Chemical oxidation is very costly and requires a catalyst for efficient removal [23]. Adsorption for the removal of toxic substances, i.e., dyes from wastewater, is the handiest [24], less expensive, more environmentally friendly [25], and the most effective and successful technique [13]. It does not cause secondary pollution with lower initial development costs, easy operation, and recoverable adsorbent material [24]. This makes them a highly desirable and affordable material worldwide for removing dyes from wastewater [9]. Therefore, the current method investigates the use of adsorption technology to remove toxic dyes from wastewater.

For adsorption, researchers have studied various types of materials ranging from natural to synthetic [26]. Natural adsorbents are readily available in nature and are much cheaper than synthetic ones [23]. Literature has reported various simple non-modified natural adsorbents for the removal of dyes, such as shrimp shells [20], eggs shells [27], peanut hull [28], olive pomace [29], spent tea leaves [30], mango bark [31], rice husk [32], coffee husks [33], peanut husk [34] and agricultural peels [35], etc. Various modified adsorbents have also been used for the removal of wastewater pollutants, such as peanut shells modified with citric acid [36], spent tea leaves modified with polyethyleneimine [37], mango seed shell activated carbon modified by Ag–Au nanoparticle [38], rice husk based magnetic nanocomposite [39], and shell treated with NaOH [40]. All these materials suffer as adsorbate recovery after absorption is almost impossible and results in the formation of sludge or may cause secondary pollution. Therefore, required a strategy to overcome this problem.

Rafiee et al. [41] worked on a pistachio shell/nanodiopside nanocomposite used for the adsorption of crystal violet dye from an aqueous solution, and 97.46% crystal violet was removed. Garg et al. [3] prepared activated carbon from peanut shells using H_3PO_4 through pyrolysis at a temperature of 650 °C under an N_2 environment which was used to remove 52 mg/g MY from wastewater. Meng et al. [42] prepared a novel polyaniline-bentonite composite adsorbent for the adsorption of anionic dyes such as MY, which has a 444.4 mg/g adsorption capacity. Saygili and Guzel [43] prepared high surface area mesoporous activated carbon from tomatoes using $ZnCl_2$ to adsorb 385 mg/g MY. Tural et al. [44] prepared glutaraldehyde cross-linked magnetic nanoparticles with chitosan nanoparticles that adsorb a maximum capacity of MY (625 mg/g).

Thus, in this study, we aim to develop carbonized pistachio magnetic nanoparticles (CPSMNPs), one of the cheap and easily available adsorbents that provide excellent textural properties, such as a high surface area for the removal of dyes from aqueous solution. Furthermore, using an external magnet, the activated carbon with magnetic nanoparticles may be easily separated from the liquids.

2. Experimental

2.1. Chemicals and Reagents

All chemicals and reagents used were of analytical grade. Ammonia solution (NH_3OH), ferric chloride hexahydrate ($FeCl_3 \cdot 6H_2O$), and MY were purchased from Sigma-Aldrich. Boric acid (H_3BO_3), phosphoric acid (H_3PO_4), Ferris-sulphate heptahydrate ($FeSO_4 \cdot 7H_2O$), sodium hydroxide (NaOH), and acetic acid (CH_3COOH) purchased from BDH laboratories, Poole, UK.

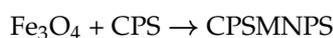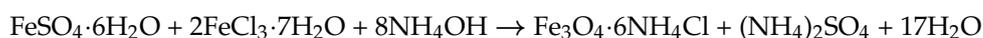### 2.2. Preparation of Adsorbent

2.2.1. Synthesis of Carbonized Pistachio Shell (CPS)

Pistachio shell (PS) obtained from the local market was washed with distilled water to remove dust and dried in an oven at 80 °C. The dried PS was ground using a ball mill and passed through a sieve to obtain a uniform particle size of less than 450 μm.

For the carbonization, 25 g powder of grounded PS was heated at 250 °C for 50 min in a stainless-steel reactor assembly with a closed lid. The lid was kept closed to prevent oxidation by fresh air. The carbonization was constantly observed to stop the formation of ash. The heating assembly was stopped when all the gases were exhausted and left with black carbonized shells. The material was cooled down to room temperature in the reactor assembly and ground into a fine powder using a pestle and mortar. The carbonized PS particle was termed CPS.

2.2.2. Preparation of Carbonized Pistachio Shell Magnetic Nanoparticles (CPSMNPs)

For the preparation of CPSMNPs, the first Fe_3O_4 nanoparticles were prepared by the co-precipitation method. For Fe_3O_4 synthesis, Fe (II) and Fe (III) salts were mixed at a molar ratio of 1:2 under an alkaline environment. $FeCl_3 \cdot 6H_2O$ (6.3 g) and $FeSO_4 \cdot 7H_2O$ (4.2 g) were dissolved separately in 100 mL of distilled water and then were mixed by vigorous stirring for 20 min. The solution was kept at 80 °C, and a black precipitate of Fe_3O_4 was obtained when 20 mL of 25% ammonium hydroxide solution was added [45]. For Fe_3O_4 impregnation on CPS, 10.5 g of CPS powder was added to the prepared solution of Fe_3O_4. The solution mixture was stirred for 1 h at 80 °C and then allowed to cool to room temperature. The obtained Fe_3O_4-impregnated CPS (Fe_3O_4-CPS) were separated by filtration, washed with distilled water, and dried in an oven for 6 h at 120 °C. The Fe_3O_4-CPS obtained was named carbonized pistachio shell magnetic nanoparticles (CPSM-NPs). CPSMNPs were checked for their magnetic property with a magnetic rod to attract magnetic nanoparticles from MY solution. The reaction that occurs during the preparation of CPSMNPs is given below:

$$FeSO_4 \cdot 6H_2O + 2FeCl_3 \cdot 7H_2O + 8NH_4OH \rightarrow Fe_3O_4 \cdot 6NH_4Cl + (NH_4)_2SO_4 + 17H_2O$$

$$Fe_3O_4 + CPS \rightarrow CPSMNPS$$

2.3. Characterization

The surface structure and morphology of PS, CPS, and CPSMNPs were determined using scanning electron microscopy (SEM, JSM5910, JEOL, Japan). The elemental composition of the materials was investigated using energy-dispersive X-rays (EDX, JEOL JDX-3532). The Brunauer–Emmett Teller (BET) specific surface areas of PS, CPS, and CPSMNPs were measured using a surface area analyzer (SAA, Micromeritics ASAP 2010) by nitrogen adsorption/desorption.

2.4. Application of CPSMNPs for Adsorption

The adsorption studies with CPSMNPs were conducted using 10 mL of 100 ppm MY solution for all the experiments. A calculated amount of the synthesized CPSMNPs were employed for MY adsorption in an aqueous solution. The systematic experiments were conducted considering the effect of pH, time, the weight of CPSMNPs, initial dye

concentration, and temperature. After adsorption, the adsorbent was removed via an external magnet, and the absorbance of the residual MY concentration was recorded via a UV–visible spectrophotometer (AE-S90-2D of A & E Lab) at 440 nm against its reference solvent. The concentration of the dye was measured before and after the adsorption to know the adsorption capability of the adsorbent CPSMNPs. The given formula was used to calculate the % adsorption of MY

$$\% \text{ Ads} = \frac{C_o - C_f}{C_o} \times 100$$

where C_o = Concentration of MY before adsorption and C_f = concentration of MY after adsorption.

The adsorption of MY was also carried out using PS and CPS, and the studies were compared with CPSMNPS following the above procedure.

3. Results and Discussion

3.1. Characterization

3.1.1. SEM Analysis

Figure 1a shows the SEM image of PS with a condensed structure and with a negligible number of pores throughout the surface. The SEM image of CPS is shown in Figure 1b. The CPS is significantly different from that of non-carbonized PS. The images of CPS depict highly porous material with inter-connected channels. The SEM image of CPS has a greater number of pores which is caused by a release of volatile gases during de-volatilization and chemical bond decomposition of the sludge matrix. Furthermore, the SEM image of CPS shows that after activation at a suitable temperature, i.e., 250 °C for 50 min in a reduced environment, small and narrow pores developed on the surface of PS when carbonized. The SEM image of CPSMNPs is shown in Figure 1c. The morphological characteristics of CPS are entirely changed after coating with Fe_3O_4, as can be seen in the figure. The SEM image of CPSMNPs reveals fine particles with an average size of 400–700 nm, resulting in a substantial increase in surface area.
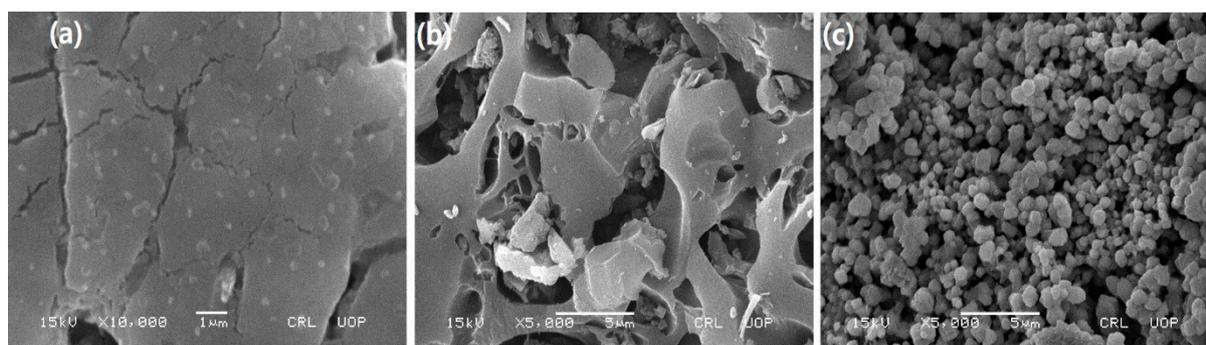

Figure 1. SEM image of (**a**) PS, (**b**) CPS, and (**c**) CPSMNPs.

3.1.2. EDX Analysis

The results obtained from EDX are given in Table 1. The EDX result obtained from PS indicates that carbon (49.05%) and chlorine (39.56%) are the principal constituents of the powder, whereas oxygen (9.40%) and iron (1.99%) was the trace element. The EDX result of CPS demonstrated that carbon (86.26%) is the essential constituent of CPS, oxygen (9.83%) is the major constituent, whereas iron (2.39%) and chlorine (1.52%) are the trace elements of the material surface. The results obtained from CPSMNPs indicate that iron (54.98%) and carbon (29.08%) are the major constituents of CPSMNPs, while oxygen (15.94%) is the most abundant constituent of CPSMNPs.

Table 1. EDX analysis, the elemental composition of PS, CPS, and CPSMNPs.

Elements	PS	CPS	CPSMNPs
Oxygen (O)	9.40	9.83	15.94
Chlorine (Cl)	39.56	1.52	0.00
Iron (Fe)	1.99	2.39	54.98
Carbon (C)	49.05	86.26	29.08

3.1.3. BET Analysis

The surface area is an essential property of a material to be used. The results of surface area analysis, i.e., BET surface area, are given in Table 2. The results show the BET surface area for PS is 26.18 m^2/g. The BET surface area for CPS calculated was 32.49 m^2/g. A substantial increase was observed as compared to PS. The large surface area indicates that activation experiments were performed satisfactorily and led to high quality. This BET surface area after impregnation of Fe$_3$O$_4$ on the surface of CPS to form CPSMNPs was further boosted to 112.58 m^2/g with excellent adsorption capabilities.

Table 2. BET surface area analysis of PS, CPS, and CPSMNPs.

Adsorbent	BET Surface Area (m^2/g)
PS	26.18
CPS	32.49
CPSMNPs	112.58

3.2. Effect of Parameters on the Adsorption of MY

The effect of various operational parameters like pH, contact time, initial dye concentration, adsorbent weight, and temperature on the % removal of MY was investigated.

3.2.1. Effect of pH

The pH plays a vital role in the adsorption of ionic dyes like MY- an anionic dye [46]. The effect of pH on the removal of MY was studied at room temperature in the pH range 2 to 12, keeping other parameters constant, i.e., contact time; 30 min, adsorbent weight; 0.1 g, initial dye concentration; 10 mL of 100 ppm MY and room temperature. The effect of pH on the MY dye removal can be explained based on the point of zero charge (PZC) on the adsorbent surface, shown in Figure 2. The PZC of the CPSMNPs adsorbent is 7.4 below this pH, the surface of the adsorbent will be positively charged due to protonation, and the positive charge increases further with low pH. Hence, the electrostatic forces get stronger between protonated CPSMNPs and negatively charged MY. Contrarily, the surface of the adsorbent is deprotonated and increases its negatively charged intensity at the pH of the solution above PZC, which is unfavorable for the adsorption of anionic dyes. Moreover, at high solution pH, more negatively charged hydroxyl ions in the solution produce a competitive effect with anionic MY, leading to a decrease in the adsorption rate [47].

The results shown in Figure 3a investigate that maximum adsorption occurred in an acidic medium, i.e., pH 2. The adsorption decreases with a rise in pH from 2 to 12. This is because the negative charge on the adsorbent's surface decreased with an increase in pH value and the electrostatic force of attraction between adsorbent and adsorbate decreased [3]. That is why % removal was optimum at pH 2, and further increasing pH decreased removal efficiency due to low protonation.
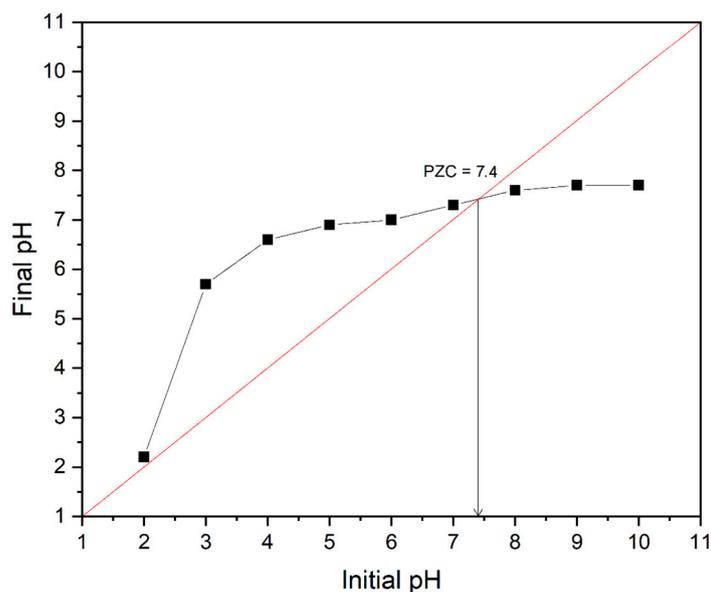
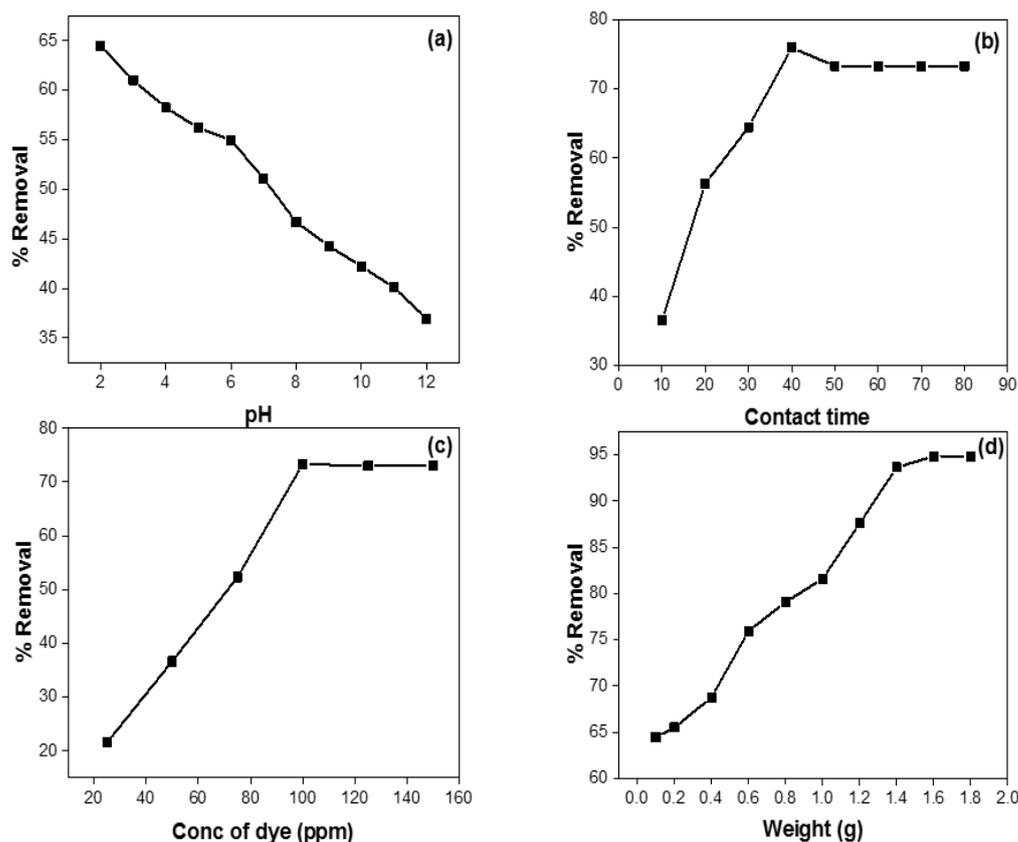**Figure 2.** Point of zero charges of CPSMNPS adsorbent.

Figure 3. Effect of various parameters on the adsorption of MY using CPSMNPs: (**a**) effect of pH; (**b**) effect of contact time; (**c**) effect of initial concentration; (**d**) effect of adsorbent dose.

3.2.2. Effect of Contact Time

The effect of contact time on the adsorption of MY was studied by varying contact time from 10 to 80 min, keeping other parameters constant, i.e., pH 2, adsorbent weight; 0.1 g, initial dye concentration; 10 mL of 100 ppm MY and room temperature. The adsorption results with the effect of contact time are shown in Figure 3b. The figure shows the adsorption increased with the increase in contact time up to 40 min, and no more increase

in the adsorption was observed by a further increase in contact time. The cause of high removal efficiency up to 40 min is due to due to the presence of more significant active sites of CPSMNPs. The active sites of adsorbent were reduced with an increase in contact time [3,9].

3.2.3. Effect of Initial Dye Concentration

Initial dye concentration depends on the relationship between dye concentration and available sites on the adsorbent surface [48]. The adsorption of MY with initial dye concentration from 25 to 150 ppm was investigated, keeping other parameters constant, i.e., the volume of dye; 10 mL, contact time 40 min, adsorbent weight; 0.1 g, and room temperature. The effect of the initial dye concentration is shown in Figure 3c. The figure show increase in initial dye concentration and increased percent removal of MY because dye molecules at initial dye concentration quickly occupy the available vacant site on the adsorbent [49]. The optimum initial concentration for MY at room temperature was 100 ppm, with a removal of 73.30%. After the optimum concentration, i.e., 100 ppm, the adsorption capacity decreased because the number of active sites was not proportional to the amount of the dye, resulting in saturation of active sites remaining in the unabsorbed MY contents [20].

3.2.4. Effect of Adsorbent Dosage

The adsorption study of MY was investigated in a research study with the effect of adsorbent dosage (weight of CPSMNPs) from 0.1 g to 1.8 g keeping other parameters constant, i.e., pH 2, contact time; 40 min, and initial dye concentration; 10 mL of 100 ppm MY and room temperature. The effect of adsorbent dosage is shown in Figure 3d. The percent removal of the dye increased with the increase in adsorbent weight, and maximum adsorption of 94.83% was recorded with 1.6 g. Initially, the increase in adsorption is due to the rise in the available active sites at the adsorbent surface [3]. A further increase in the adsorbent weight has no significant and effective adsorption due to the saturation behavior of adsorption sites [50].

3.3. Comparison of Adsorption Studies Using PS and CPS with CPSMNPs

The adsorption of MY was also carried out using PS and CPS, and the data were compared with that of CPSMNPs using the same effecting parameters. The comparison studies are given in Table 3. The studies revealed that the removal performance of PS was $63.32 \pm 6.36\%$, which is much lower than CPS and CPSMNPS. The removal performance in CPS and CPSMNPs was almost the same, i.e., $94.78 \pm 7.32\%$ and $94.83 \pm 1.21\%$, respectively. There was a high fluctuation in the results while performing the adsorptive removal of MY using PS and CPS, indicated by their high standard deviation value. This is attributed to the incomplete removal of adsorbent either by filtration and/or centrifugation. The removal of adsorbent is very hard in the case of CPS, which causes high fluctuations in the results. On the other hand, the complete removal of CPSMNPs is highly easy, i.e., the application of an external magnet facilitates the removal.

Table 3. Comparison of PS and CPS with CPSMNPs for the adsorption of MY using the same effecting parameters.

Adsorbent	%Removal of MY	SD
PS	63.32	6.36
CPS	94.78	7.32
CPSMNPs	94.83	1.21

3.4. Adsorption Isotherms

Adsorption isotherm models were used to design the adsorption phenomena. The amount of dye adsorbed on the sorbent and these isotherms determine the dye concentra-

tion in the solution at equilibrium. Freundlich and Langmuir's isotherm models were used to investigate the isotherm of dye adsorption on the sorbent. The Freundlich isotherm is used for non-ideal adsorption on heterogeneous surfaces and is expressed by the following Equation (1) [51]:

$$q_e = K_F C_e^{\frac{1}{n}} \tag{1}$$

The linear form of the Freundlich equation is given (2) [51]:

$$\log q_e = \log K_F + \frac{1}{n} \log C_e \tag{2}$$

where K_F is the Freundlich sorption isotherm constant (mg g^{-1}), $1/n$ (g L^{-1}) is a measure of the adsorption intensity, q_e is the amount sorption (mg g^{-1}), and C_e is the equilibrium concentration (μg mL^{-1}).

Langmuir isotherm model is used for monolayer sorption on a homogeneous surface and is represented by the following equation:

$$q_e = \frac{K_L C_e}{1 + a_L C_e} \tag{3}$$

Their linear form is expressed in the following form [52]:

$$\frac{C_e}{q_e} = \frac{1}{K_L} + \frac{a_L C_e}{K_L} \tag{4}$$

where C_e is equilibrium concentration (μg mL^{-1}), q_e is the amount of solute sorption per gram of sorbent; K_L and a_L are the Langmuir sorption model constants and are related to the maximum capacity (L g^{-1}) and bonding strength (L mg^{-1}), respectively. The theoretical monolayer capacity is Q_o and is numerically equal to K_L (L g^{-1})

Figure 4a,b shows the results of these isotherms, respectively. Table 4 shows the constant parameters for this isotherm, which were calculated from the slope and intercept of the linear form of their respective equations. Because the n value of the Freundlich model is less than unity, dye is not adsorbed favorably on CPSMNPs. The linear form of the Langmuir isotherm was used to calculate the maximum adsorption capacity, which was found to be 97 mg g^{-1}. Because of the high correlation coefficient ($R^2 = 0.9947$), it can be concluded that the sorption data of dyes on CPSMNPs best fits into the Langmuir isotherm model.
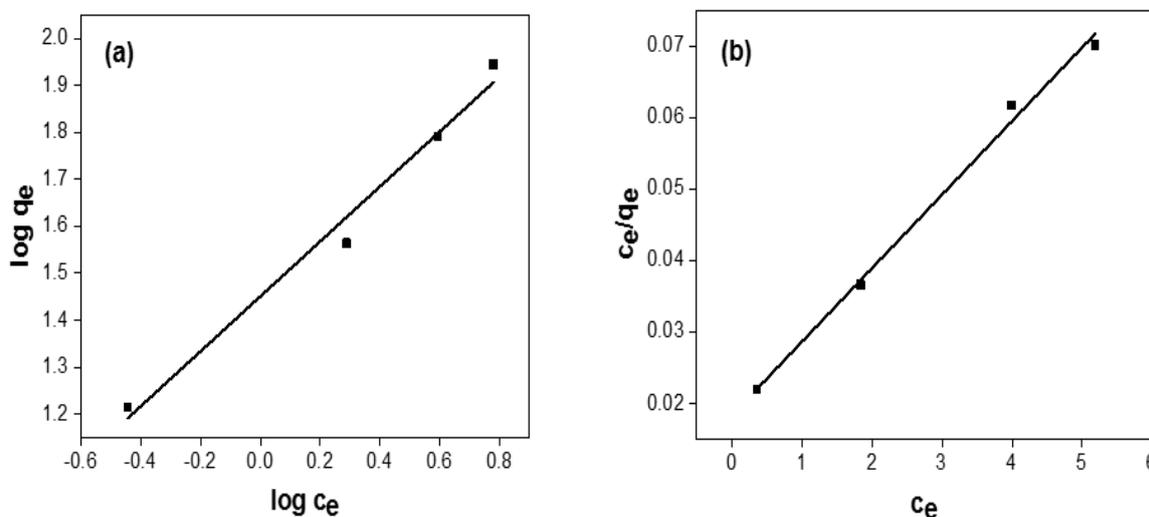

Figure 4. (**a**) Freundlich isotherm; (**b**) Langmuir isotherm for sorption of dyes using CPSMNPs.

Table 4. Freundlich and Langmuir isotherm constants for MY adsorption on CPSMNPs.

Isotherm	Parameters	Values
Freundlich isotherm	K_F (mg g^{-1})	28.24
	N	0.946
	1/n	0.5847
	R^2	0.983
Langmuir isotherm	a_L (L mg^{-1})	0.56
	K_L (L g^{-1})	54.6
	Q_o (mg g^{-1})	97
	R^2	0.9947

3.5. Kinetic Studies

Adsorption kinetics provides the adsorption of solute in liquid/solid systems due to the solid adsorbent and identifies the adsorption capacity of the solid system [11]. The data from kinetics studies were obtained using optimized parameters. The data of the current study were fitted in the pseudo-first-order kinetics model Equation (5) [3] and pseudo-second-order kinetics model Equation (6) [53].

$$Log(q_e - q_e) = logq_e - \frac{K_1 t}{2.303} \tag{5}$$

$$\frac{t}{q_t} = \frac{1}{q_e} + \frac{1}{K_2 \times q_e^2} \tag{6}$$

where q_e and q_t are the amounts of MY in mg/g. K_1 and K_2 kinetic models are constant for pseudo-first and pseudo-second order, respectively.

A linear plot of log $(q_e - q_t)$ versus t for the pseudo-first-order model was used to calculate R^2, K_1, and qe, shown in Figure 5a, and the t/q_e versus t plot for pseudo-second-order was used to calculate K_2, q_e and R^2 in Figure 5b. The results of both plots showed that the adsorption of MY follows the pseudo-second-order kinetics model because of the closeness of the theoretical and experimental values of q_e shown in Table 5.
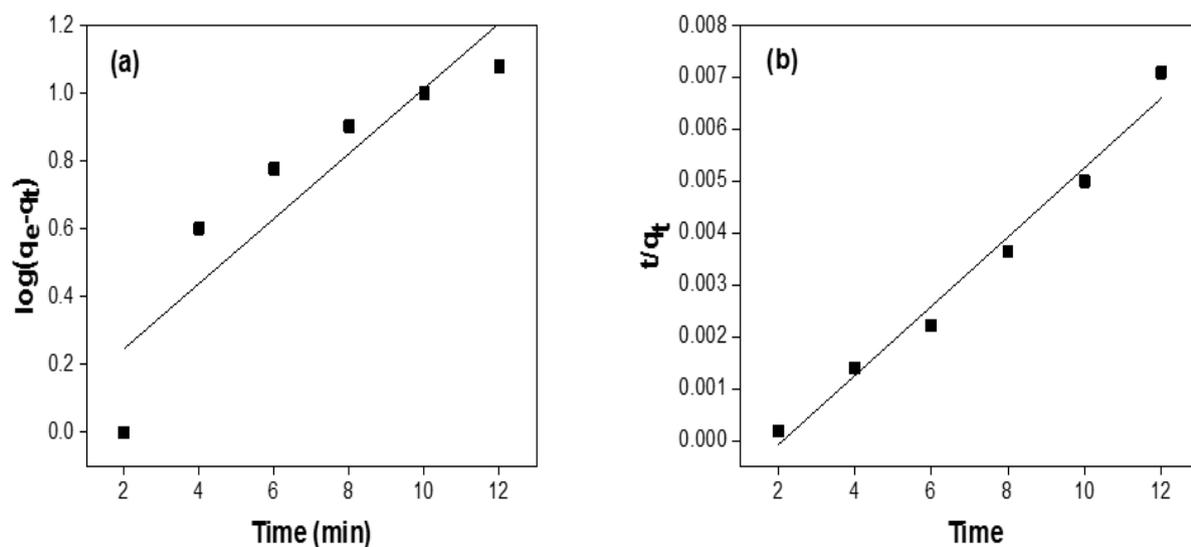

Figure 5. (**a**) Pseudo-first-order kinetics plot; (**b**) pseudo-second-order kinetics plot.

Table 5. Kinetic data for the adsorption of MY on CPSMNPs.

Kinetic Model	Parameters	Values
	q_e (exp)	3433.96
Pseudo first order	$K1$ (min^{-1})	0.2208
	q_e calc (mg g^{-1})	1.1365
	R^2	0.8297
	C	0.0556
Pseudo second order	$K2$ (min^{-1})	0.0003
	q_e calc (mg g^{-1})	1428.57
	q_e^2 calc (mg g^{-1})	2,040,816.3
	R^2	0.9803
	C	0.0014

3.6. Thermodynamics Studies

The study of thermodynamics assumes that the energy in an isolated system cannot be lost or gained when the entropy change is the driving force. Thermodynamic parameters were calculated for the determination of the sorption process that either occurs spontaneously or not. The change in free energy ($\Delta G°$) [54], enthalpy ($\Delta H°$), and entropy ($\Delta S°$) [55] of the sorption process was calculated by using the following equations [37]:

$$K_D = \frac{q_e}{C_e} \tag{7}$$

$$\Delta G° = -RT\ln K_D \tag{8}$$

$$\ln K_D = -\frac{\Delta G°}{RT} = -\frac{\Delta H°}{RT} + \frac{\Delta S°}{R} \tag{9}$$

where K_D is the distribution constant, q_e is the amount of metal ion sorption (mg g^{-1}) at equilibrium, and C_e is the equilibrium concentration (μg mL^{-1}).

The values of $\ln K_D$ are plotted against $1/T$. The results are shown in Figure 6. K_D, $\Delta G°$, $\Delta H°$, and $\Delta S°$ values for MY sorption on CPSMNPs were calculated using Equations (7)–(9) in Table 6. An exothermic sorption process was indicated by the negative value for enthalpy change ($\Delta H°$). The positive value of entropy ($\Delta S°$) indicated CPSMNP affinity for MY adsorption, whereas the negative value of $\Delta G°$ indicated that the sorption process is spontaneous at the temperature range investigated.
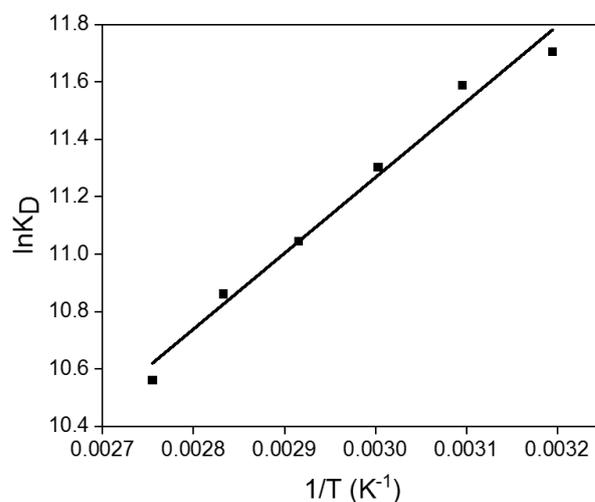

Figure 6. The plot of lnKD versus 1/T for estimation of thermodynamic parameters for MY sorption on CPSMNPs.

Table 6. Thermodynamic studies for the sorption of MY on CPSMNPs.

Temperature (K)	$-\Delta G°$ (kJ mol^{-1})	$\Delta H°$ (kJ mol^{-1})	$\Delta S°$ (kJ K^{-1})
313	30.430	−23.670	0.022
323	31.091	-	-
333	31.831	-	-
343	31.490	-	-
353	31.880	-	-
363	31.570	-	-

3.7. Comparison of the Current Study with Literature

The present study compared the literature-reported methods for the adsorption of MY using CPSMNPs. The adsorption capacity of CPSMNPs in the present study is much higher compared to that of literature-reported methods [11,12,20,42,44,56–58]. The comparison of the present study with literature-reported methods is shown in Table 7.

Table 7. Comparison of adsorbent for the adsorption of MY of the present study with literature-reported methods.

Adsorbents	Adsorption Capacity (mg.g^{-1})	Time (min)	pH	Reference
Leaves *Prosopis juliflora*	26.00	150	2	[11]
Mg-Fe-NO$_3$ Layered double hydroxide	42.72	120	6	[56]
Pilot-scale produced super-activated carbon	937.00	60	3	[57]
Peanut shell-based activated carbon	52.00	150	2	[3]
Shrimp shell	69.31	75	5	[20]
Bovine serum albumin-modified rice husk silica	80.00	120	5	[58]
Saw dust carbon	183.00	400	3	[12]
Cross linked magnetic biosorbent	385.00	240	6	[44]
Polyaniline-bentonite composite (Bent)	444.44	240	7	[42]
CPSMNPs	1428.00	40	2	Present study

4. Conclusions

The cost-effective adsorbents of CPSMNPs were efficiently synthesized and used for MY adsorption. The SEM image of CPSMNPs reveals fine particles with an average size of 400–700 nm with a substantially increased surface area of 112.58 m^2/g compared to that of PS (26.18 m^2/g) and CPS (32.49 m^2/g). The EDX analysis confirmed the carbonization of PS to CPS and the successful impregnation of Fe$_3$O$_4$ nanoparticles. CPSMNPs showed excellent adsorption efficiency, i.e., 94% for the removal of MY of 10 mL of 100 ppm MY at pH 2, 0.6 g adsorbent dosage, 40 min contact time, and room temperature. Kinetics data fit pseudo-second-order kinetics. The Langmuir isotherm better represented the equilibrium data. The thermodynamics studies showed the sorption process was spontaneous. This study investigates that the synthesized nanoparticles have good texture and can be used as a special adsorbent for the adsorption of wastewater pollutants like MY.

References

1. Jan, S.U.; Ahmad, A.; Khan, A.A.; Melhi, S.; Ahmad, I.; Sun, G.; Chen, C.-M.; Ahmad, R. Removal of azo dye from aqueous solution by a low-cost activated carbon prepared from coal: Adsorption kinetics, isotherms study, and DFT simulation. *Environ. Sci. Pollut. Res.* **2020**, *28*, 10234–10247. [CrossRef] [PubMed]
2. Sharma, G.; Kumar, A.; Naushad, M.; Kumar, A.; Al-Muhtaseb, A.H.; Dhiman, P.; Ghfar, A.A.; Stadler, F.J.; Khan, M. Photoremediation of toxic dye from aqueous environment using monometallic and bimetallic quantum dots-based nanocomposites. *J. Clean. Prod.* **2018**, *172*, 2919–2930. [CrossRef]
3. Garg, D.; Kumar, S.; Sharma, K.; Majumder, C. Application of waste peanut shells to form activated carbon and its utilization for the removal of Acid Yellow 36 from wastewater. *Groundw. Sustain. Dev.* **2019**, *8*, 512–519. [CrossRef]
4. Gupta, V.K. Suhas Application of low-cost adsorbents for dye removal—A review. *J. Environ. Manag.* **2009**, *90*, 2313–2342. [CrossRef]
5. Adegoke, K.A.; Bello, O.S. Dye sequestration using agricultural wastes as adsorbents. *Water Resour. Ind.* **2015**, *12*, 8–24. [CrossRef]
6. Khan, T.A.; Nazir, M.; Khan, E.A. Adsorptive removal of rhodamine B from textile wastewater using water chestnut (*Trapa natans* L.) peel: Adsorption dynamics and kinetic studies. *Toxicol. Environ. Chem.* **2013**, *95*, 919–931. [CrossRef]
7. Banerjee, P.; Sau, S.; Das, P.; Mukhopadhayay, A. Optimization and modelling of synthetic azo dye wastewater treatment using Graphene oxide nanoplatelets: Characterization toxicity evaluation and optimization using Artificial Neural Network. *Ecotoxicol. Environ. Saf.* **2015**, *119*, 47–57. [CrossRef]
8. Sayğılı, H.; Güzel, F.; Önal, Y. Conversion of grape industrial processing waste to activated carbon sorbent and its performance in cationic and anionic dyes adsorption. *J. Clean. Prod.* **2015**, *93*, 84–93. [CrossRef]
9. Şentürk, I.; Alzein, M. Adsorptive removal of basic blue 41 using pistachio shell adsorbent—Performance in batch and column system. *Sustain. Chem. Pharm.* **2020**, *16*, 100254. [CrossRef]
10. Delnavaz, M.; Mofrad, Z.K. Nano zerovalent iron (NZVI) adsorption performance on acidic dye 36 removal: Optimization of effective factors, isotherm and kinetic study. *Environ. Prog. Sustain. Energy* **2019**, *39*, e13349. [CrossRef]
11. Thirunavukkarasu, A.; Muthukumaran, K.; Nithya, R. Adsorption of acid yellow 36 onto green nanoceria and amine functionalized green nanoceria: Comparative studies on kinetics, isotherm, thermodynamics, and diffusion analysis. *J. Taiwan Inst. Chem. Eng.* **2018**, *93*, 211–225. [CrossRef]
12. Malik, P. Use of activated carbons prepared from sawdust and rice-husk for adsorption of acid dyes: A case study of Acid Yellow 36. *Dye. Pigment.* **2003**, *56*, 239–249. [CrossRef]
13. Chiou, M.-S.; Chuang, G.-S. Competitive adsorption of dye metanil yellow and RB15 in acid solutions on chemically cross-linked chitosan beads. *Chemosphere* **2006**, *62*, 731–740. [CrossRef] [PubMed]
14. Ponnusami, V.; Gunasekar, V.; Srivastava, S. Kinetics of methylene blue removal from aqueous solution using gulmohar (*Delonix regia*) plant leaf powder: Multivariate regression analysis. *J. Hazard. Mater.* **2009**, *169*, 119–127. [CrossRef]
15. Sathishkumar, P.; Arulkumar, M.; Palvannan, T. Utilization of agro-industrial waste Jatropha curcas pods as an activated carbon for the adsorption of reactive dye Remazol Brilliant Blue R (RBBR). *J. Clean. Prod.* **2012**, *22*, 67–75. [CrossRef]
16. Mittal, A.; Gupta, V.; Malviya, A.; Mittal, J. Process development for the batch and bulk removal and recovery of a hazardous, water-soluble azo dye (Metanil Yellow) by adsorption over waste materials (Bottom Ash and De-Oiled Soya). *J. Hazard. Mater.* **2008**, *151*, 821–832. [CrossRef]
17. Attia, A.A.; Rashwan, W.E.; Khedr, S.A. Capacity of activated carbon in the removal of acid dyes subsequent to its thermal treatment. *Dye. Pigment.* **2006**, *69*, 128–136. [CrossRef]
18. Chen, X.; Lim, J.F.; Xu, Y.; Hong, L. Operating conditions and feed composition on filtering emulsified oil using ceramic-hybrid membrane. *Ceram. Int.* **2016**, *42*, 17101–17109. [CrossRef]
19. Tan, K.B.; Vakili, M.; Horri, B.A.; Poh, P.E.; Abdullah, A.Z.; Salamatinia, B. Adsorption of dyes by nanomaterials: Recent developments and adsorption mechanisms. *Sep. Purif. Technol.* **2015**, *150*, 229–242. [CrossRef]
20. Ramadhani, P.; Chaidir, Z.; Zilfa, Z.; Tomi, Z.B.; Rahmiarti, D.; Zein, R. Shrimp shell (*Metapenaeus monoceros*) waste as a low-cost adsorbent for metanil yellow dye removal in aqueous solution. *Desalination Water Treat.* **2020**, *197*, 413–423. [CrossRef]
21. Khoshhesab, Z.M.; Souhani, S. Adsorptive removal of reactive dyes from aqueous solutions using zinc oxide nanoparticles. *J. Chin. Chem. Soc.* **2018**, *65*, 1482–1490. [CrossRef]

22. Velusamy, S.; Roy, A.; Sundaram, S.; Mallick, T.K. A Review on Heavy Metal Ions and Containing Dyes Removal Through Graphene Oxide-Based Adsorption Strategies for Textile Wastewater Treatment. *Chem. Rec.* **2021**, *21*, 1570–1610. [CrossRef] [PubMed]

23. Katheresan, V.; Kansedo, J.; Lau, S.Y. Efficiency of various recent wastewater dye removal methods: A review. *J. Environ. Chem. Eng.* **2018**, *6*, 4676–4697. [CrossRef]

24. Shah, J.; Jan, M.R.; Khitab, F. Sonophotocatalytic degradation of textile dyes over Cu impregnated ZnO catalyst in aqueous solution. *Process Saf. Environ. Prot.* **2018**, *116*, 149–158. [CrossRef]

25. Mohan, D.; Pittman, C.U., Jr. Activated carbons and low cost adsorbents for remediation of tri-and hexavalent chromium from water. *J. Hazard. Mater.* **2006**, *137*, 762–811. [CrossRef] [PubMed]

26. Nagappan, S.; Jeon, Y.; Park, S.S.; Ha, C.-S. Hexadecyltrimethylammonium Bromide Surfactant-Supported Silica Material for the Effective Adsorption of Metanil Yellow Dye. *ACS Omega* **2019**, *4*, 8548–8558. [CrossRef]

27. Slimani, R.; El Ouahabi, I.; Abidi, F.; El Haddad, M.; Regti, A.; Laamari, M.R.; El Antri, S.; Lazar, S. Calcined eggshells as a new biosorbent to remove basic dye from aqueous solutions: Thermodynamics, kinetics, isotherms and error analysis. *J. Taiwan Inst. Chem. Eng.* **2014**, *45*, 1578–1587. [CrossRef]

28. Gong, R.; Sun, Y.; Chen, J.; Liu, H.; Yang, C. Effect of chemical modification on dye adsorption capacity of peanut hull. *Dye. Pigment.* **2005**, *67*, 175–181. [CrossRef]

29. Akar, T.; Tosun, I.; Kaynak, Z.; Ozkara, E.; Yeni, O.; Sahin, E.N.; Akar, S.T. An attractive agro-industrial by-product in environmental cleanup: Dye biosorption potential of untreated olive pomace. *J. Hazard. Mater.* **2009**, *166*, 1217–1225. [CrossRef]

30. Hameed, B. Spent tea leaves: A new non-conventional and low-cost adsorbent for removal of basic dye from aqueous solutions. *J. Hazard. Mater.* **2009**, *161*, 753–759. [CrossRef]

31. Srivastava, R.; Rupainwar, D. A comparative evaluation for adsorption of dye on Neem bark and mango bark powder. *Indian J. Chem. Technol.* **2011**, *18*, 67–75.

32. Vadivelan, V.; Kumar, K.V. Equilibrium, kinetics, mechanism, and process design for the sorption of methylene blue onto rice husk. *J. Colloid Interface Sci.* **2005**, *286*, 90–100. [CrossRef] [PubMed]

33. Oliveira, L.S.; Franca, A.S.; Alves, T.M.; Rocha, S.D. Evaluation of untreated coffee husks as potential biosorbents for treatment of dye contaminated waters. *J. Hazard. Mater.* **2008**, *155*, 507–512. [CrossRef] [PubMed]

34. Sadaf, S.; Bhatti, H.N. Batch and fixed bed column studies for the removal of Indosol Yellow BG dye by peanut husk. *J. Taiwan Inst. Chem. Eng.* **2014**, *45*, 541–553. [CrossRef]

35. Anastopoulos, I.; Kyzas, G.Z. Agricultural peels for dye adsorption: A review of recent literature. *J. Mol. Liq.* **2014**, *200*, 381–389. [CrossRef]

36. Wang, P.; Ma, Q.; Hu, D.; Wang, L. Adsorption of methylene blue by a low-cost biosorbent: Citric acid modified peanut shell. *Desalin. Water Treat.* **2016**, *57*, 10261–10269. [CrossRef]

37. Wong, S.; Tumari, H.H.; Ngadi, N.; Mohamed, N.B.; Hassan, O.; Mat, R.; Amin, N.A.S. Adsorption of anionic dyes on spent tea leaves modified with polyethyleneimine (PEI-STL). *J. Clean. Prod.* **2018**, *206*, 394–406. [CrossRef]

38. Okeowo, I.O.; Balogun, E.O.; Ademola, A.J.; Alade, A.O.; Afolabi, T.J.; Dada, E.O.; Farombi, A.G. Adsorption of Phenol from Wastewater Using Microwave-Assisted Ag–Au Nanoparticle-Modified Mango Seed Shell-Activated Carbon. *Int. J. Environ. Res.* **2020**, *14*, 215–233. [CrossRef]

39. Luyen, N.T.; Linh, H.X.; Huy, T.Q. Preparation of Rice Husk Biochar-Based Magnetic Nanocomposite for Effective Removal of Crystal Violet. *J. Electron. Mater.* **2019**, *49*, 1142–1149. [CrossRef]

40. Khan, M.A.; Al Othman, Z.A.; Kumar, M.; Ola, M.S.; Siddique, M.R. Biosorption potential assessment of modified pistachio shell waste for methylene blue: Thermodynamics and kinetics study. *Desalination Water Treat.* **2014**, *56*, 146–160. [CrossRef]

41. Rafiee, A.; Nasab, S.G.; Teimouri, A. Synthesis and characterization of pistachio shell/nanodiopside nanocomposite and its application for removal of Crystal Violet dye from aqueous solutions using central composite design. *Int. J. Environ. Anal. Chem.* **2019**, *100*, 1624–1649. [CrossRef]

42. Meng, F.; Wang, L.; Pei, M.; Guo, W.; Liu, G. Adsorption of metanil yellow from aqueous solution using polyaniline-bentonite composite. *Colloid Polym. Sci.* **2017**, *295*, 1165–1175. [CrossRef]

43. Sayğılı, H.; Güzel, F. High surface area mesoporous activated carbon from tomato processing solid waste by zinc chloride activation: Process optimization, characterization and dyes adsorption. *J. Clean. Prod.* **2016**, *113*, 995–1004. [CrossRef]

44. Tural, S.; Tarhan, T.; Tural, B. Removal of hazardous azo dye Metanil Yellow from aqueous solution by cross-linked magnetic biosorbent; equilibrium and kinetic studies. *Desalination Water Treat.* **2015**, *57*, 13347–13356. [CrossRef]

45. Khan, M.; Naseer, S.; Khan, M.; Nazir, R.; Badshah, A.; Adnan Shujah, S.; Parveen, A. Magnetic solid-phase extraction of Cd (II) from water samples using magnetic nanoparticles impregnated walnut shells powder (MNPS-WSP). *Desalination Water Treat.* **2021**, *228*, 286–296. [CrossRef]

46. Shokoohi, R.; Torkshavand, Z.; Mahmoudi, M.M.; Behgoo, A.M.; Ghaedrahmati, E.; Hosseini, F.M. Effective Removal of Azo Dye Reactive Blue 222 from Aqueous Solutions Using Modified Magnetic Nanoparticles with Sodium Alginate/Hydrogen Peroxide. *Environ. Prog. Sustain. Energy* **2018**, *38*, S205–S213. [CrossRef]

47. Nordin, A.H.; Wong, S.; Ngadi, N.; Zainol, M.M.; Latif, N.A.F.A.; Nabgan, W. Surface functionalization of cellulose with polyethyleneimine and magnetic nanoparticles for efficient removal of anionic dye in wastewater. *J. Environ. Chem. Eng.* **2020**, *9*, 104639. [CrossRef]

48. Regti, A.; Laamari, M.R.; Stiriba, S.-E.; El Haddad, M. Removal of Basic Blue 41 dyes using Persea americana-activated carbon prepared by phosphoric acid action. *Int. J. Ind. Chem.* **2016**, *8*, 187–195. [CrossRef]

49. Salari, N.M.A.; Tehrani, R.; Motamedi, M. Zeolite modification with cellulose nanofiber/magnetic nanoparticles for the elimination of reactive red 198. *Int. J. Biol. Macromol.* **2021**, *176*, 342–351. [CrossRef]

50. Aydın, H.; Baysal, G. Adsorption of acid dyes in aqueous solutions by shells of bittim (*Pistacia khinjuk* Stocks). *Desalination* **2006**, *196*, 248–259. [CrossRef]

51. Benjelloun, M.; Miyah, Y.; Evrendilek, G.A.; Zerrouq, F.; Lairini, S. Recent Advances in Adsorption Kinetic Models: Their Application to Dye Types. *Arab. J. Chem.* **2021**, *14*, 103031. [CrossRef]

52. Nejadshafiee, V.; Islami, M.R. Adsorption capacity of heavy metal ions using sultone-modified magnetic activated carbon as a bio-adsorbent. *Mater. Sci. Eng. C* **2019**, *101*, 42–52. [CrossRef] [PubMed]

53. Garg, D.; Majumder, C.B.; Kumar, S.; Sarkar, B. Removal of Direct Blue-86 dye from aqueous solution using alginate encapsulated activated carbon (PnsAC-alginate) prepared from waste peanut shell. *J. Environ. Chem. Eng.* **2019**, *7*, 103365. [CrossRef]

54. Sivashankar, R.; Sathya, A.; Vasantharaj, K.; Sivasubramanian, V. Magnetic composite an environmental super adsorbent for dye sequestration—A review. *Environ. Nanotechnol. Monit. Manag.* **2014**, *1–2*, 36–49. [CrossRef]

55. Shan, R.R.; Yan, L.G.; Yang, K.; Yu, S.J.; Hao, Y.F.; Yu, H.Q.; Du, B. Magnetic Fe3O4/MgAl-LDH composite for effective removal of three red dyes from aqueous solution. *Chem. Eng. J.* **2014**, *252*, 38–46. [CrossRef]

56. Nejati, K.; Rezvani, Z.; Mansurfar, M.; Mirzaee, A.; Mahkam, M. Adsorption of Metanil Yellow Azoic Dye from Aqueous Solution onto Mg-Fe-NO3 Layered Double Hydroxide. *Z. Für Anorg. Allg. Chem.* **2011**, *637*, 1573–1579. [CrossRef]

57. Sawant, S.Y.; Pawar, R.R.; Senthilkumar, S.; Somani, R.S.; Cho, M.H.; Bajaj, H.C. Pilot-scale produced super activated carbon with a nanoporous texture as an excellent adsorbent for the efficient removal of metanil yellow. *Powder Technol.* **2018**, *333*, 243–251. [CrossRef]

58. Zein, R.; Tomi, Z.B.; Fauzia, S.; Zilfa, Z. Modification of rice husk silica with bovine serum albumin (BSA) for improvement in adsorption of metanil yellow dye. *J. Iran. Chem. Soc.* **2020**, *17*, 2599–2612. [CrossRef]